INSTITUTE OF PHYSICS PUBLISHING JOURNAL OF OPTICS A: PURE AND APPLIED OPTICS
J. Opt. A: Pure Appl. Opt. **8** (2006) 415–422 doi:10.1088/1464-4258/8/5/008

Monte Carlo simulation for modulated pulse bathymetric light detecting and ranging systems

Jun Liang[1], Kecheng Yang[1], Min Xia[1], Xiaohui Zhang[2], Xuanhua Lei[2], Yi Zheng[1] and Dan Tan[3]

[1] State Key Laboratory of Laser Technology, Huazhong University of Science and Technology, Wuhan, Hubei 430074, People's Republic of China
[2] Navy Engineering University, Wuhan, Hubei 430033, People's Republic of China
[3] College of Electrical and Electronic Engineering, Huazhong University of Science and Technology, Wuhan, Hubei 430074, People's Republic of China

E-mail: kcyang@hust.edu.cn

Received 23 January 2006, accepted for publication 3 March 2006
Published 23 March 2006
Online at stacks.iop.org/JOptA/8/415

Abstract
A modulated light detecting and ranging (LIDAR) system has been developed to improve the detection of underwater targets. To study this detection scheme, this paper proposes a Monte Carlo simulation method for modulated pulse LIDAR systems. First, a Monte Carlo model is developed to simulate modulated pulse propagation in sea water. Second, a receiving system model is emulated with advanced signal processing tools like Fourier transform, cross-correlation and filtering. The simulation program based on the model is realized. This program is capable of predicting experimental results and helping in the design of more advanced transmitter and receiver configurations as various parameters of the environment, modulation and geometry are taken into account in our design. The calculations of backscattering frequency responses with different attenuation coefficients exhibit the low-pass filter-like response of backscattering. The modulated LIDAR results for a target depth of 5 m and attenuation coefficient of $c = 0.67$ and 0.85 m^{-1} are also computed. It is validated that the modulation approach can suppress volume backscattering clutter and can enhance the target contrast. Furthermore, comparisons with reported experimental results indicate the feasibility of the simulation model.

Keywords: LIDAR, modulation, Monte Carlo method, backscattering

1. Introduction

Blue–green LIDAR (light detecting and ranging) has been used for tracking underwater objects and mapping the ocean bottom. A typical application is a bathymetric LIDAR system, which infers the water depth in coastal regions by transmitting a laser pulse into the water and monitoring the return signal from the sea bottom interface. While the transmitted optical signal is propagating through the water medium, it is spread and attenuated by absorption and scattering. In particular, volume backscattering clutter severely reduces the system sensitivity and underwater target contrast. These currently limit the performance of LIDAR systems.

In response to this shortcoming, a detection scheme has been proposed by using radiofrequency modulation on short optical pulses [1–4]. This scheme combines the coherent detection of microwave radar and underwater transmission capability of LIDAR. Physical justification of this technique is found in the existence of the low-pass frequency response of scattering in ocean water. A theoretical model of this frequency response has been proposed by Mullen *et al* [5]. A laboratory tank experimental study of seawater transfer functions deduced

from backscattering measurements for various water turbidities has been carried out by Pellen *et al* [6]. In our paper, Monte Carlo simulation gives the water impulse responses from which the frequency responses are computed by taking the Fourier transform.

To verify this detection scheme, laboratory experiments based on an optical fibre-based ocean mass simulator (OMS) [1, 4, 5] and a water tank [7] were completed. These laboratory experiments established the significant advantages of the new approach. However, complex mechanisms governing the transport of light through ocean water cannot be totally represented in the laboratory environment.

To validate the benefits and understand the limitations of the detection scheme in the actual ocean environment, a field test was conducted from a tower located approximately 1 mile from the shore of the Atlantic Undersea Test and Evaluation Center (AUTEC) on Andros Island, Bahamas [8–10]. This test enhanced conventional measurements with moderate cost but was still faced with the problems associated with spatial and temporal variability and limitations including invariant water quality, shallow water depth, and a low platform altitude. These resulted in a deviation from the aerial system. Furthermore, the challenges in developing components capable of high-speed light modulation and detection limit our ability to fully investigate the potential of the modulated approach in various environments and scenarios. These are the reasons why we are currently designing and realizing computer simulations to evaluate the aerial modulated LIDAR system performance.

Propagation of light in homogeneous scattering media can be mathematically described by the radiative transfer equation. The theoretical model for modulated light beam propagation was developed by Mullen *et al* [11]. However, accurate analytical solutions using approximate methods such as the multi-component method and small angle diffusion approximation [11] are limited to particular cases. A technique is needed for more realistic investigations of airborne modulated LIDAR system measurements over a wide range of environmental conditions, as well as for various transmitter/receiver configurations. The Monte Carlo method can be applied to any problem if one knows the probability for each step in a sequence of events and desires the probability of the total of all possible events [12]. In particular, it does not require extra simplifying assumptions compared with the radiative transport equation. Thus, the Monte Carlo method is suitable for studying problems in oceanic radiative transfer. There have been many examples of Monte Carlo studies of radiative transfer in scattering media [12–17]. Moreover, this method has the ability to deal with any situation regarding the emission–reception geometry and the scattering characteristics of the medium. Therefore, this study chose the Monte Carlo method to simulate modulated pulse bathymetric LIDAR systems.

2. Design of Monte Carlo radiative transfer model

A modulated pulse bathymetric LIDAR system, as shown in figure 1, contains these principal elements: the optical transmitter, the receiver, and the signal processor. The transmitter consists of a pulsed laser, a modulator driver and a modulator. In figure 1, the section between points l_1 and l_2 is the basic bathymetric LIDAR system. The pulsed laser generates a high-power, blue–green optical pulse, which penetrates deep into the sea water, and the return signal from the sea floor is captured by a receiver which includes a photodetector. For the application of the modulation detection scheme, the transmitter produces a radiofrequency-modulated optical pulse by superimposing a microwave envelope on the optical carrier at point m_1. The microwave signal is then transported through the water by an optical carrier. The reflected optical signal, with the microwave envelope, is detected by the receiver. There is an additional step other than photodetection in the basic LIDAR system, that is, the output of the photodetector is finally subjected to coherent signal processing. At point m_2, the result processed is obtained.

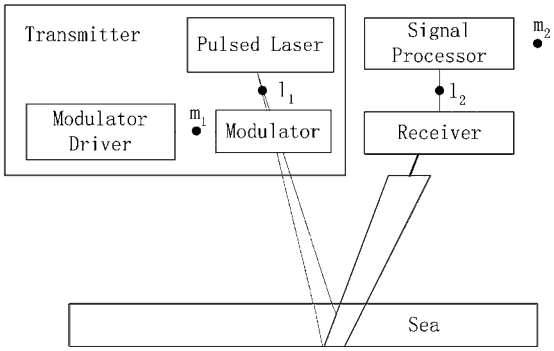

Figure 1. Block diagram of a modulated pulse bathymetric LIDAR system.

The primary objective of our model is to simulate the modulated pulse bathymetric LIDAR system. The key to the simulation for this system is the Monte Carlo radiative transfer model for modulated pulses.

To reduce the complexity of the simulation, several simplifying assumptions are introduced. First, as is customary in LIDAR studies, we set the time reference at the arrival of the surface return. Second, atmospheric effects are not considered. Third, the spot size and divergence of the emitted laser are negligible. Fourth, the ocean surface is assumed smooth. The building process of the model can be divided into three stages. The first stage is to set up the simplest Monte Carlo model for propagation of a 0-pulse-width light pulse in the atmosphere–ocean system. In the second stage, called a simulation model for propagation of a realistic pulse in atmosphere–ocean system, the influence of pulse width on the simulation is taken into account. The third stage, which is based on the second step, is to simulate the propagation of modulated pulses.

2.1. Model for propagation of a 0-pulse-width light pulse

In this stage, a pulse that is supposed to have no width is transmitted into the water medium, where it is attenuated due to absorption and scattering, as it propagates to the ocean bottom. It is also reflected from the ocean bottom and randomly backscattered from the ocean mass. The basic model has actually been developed in several early studies [13–17].

In our simulation each original photon is assigned a statistical weight such as 1. Photons are generated at the

airborne transmitter, and without atmosphere effects, they vertically enter the atmosphere–ocean interface at which reflection and refraction happen. The reflection will be eliminated from received signals in order to turn our attention to backscattered light and sea floor reflection.

Then the path of each photon in water is traced. This technique uses a computer to generate random numbers that correspond to the direction and length of each step in the random walk. First, random numbers uniformly distributed in the interval [0, 1] are obtained from an algorithm for generating pseudorandom numbers. These random numbers are then transformed so that they are distributed according to probability density functions derived from the basic scattering and absorption properties of the medium. The random path length between two successive scattering events is deduced from the Beer–Lambert law [6]. At each collision point the statistical weight of the photon is also adjusted according to the single-scattering albedo $\omega = b/c$ or $\omega = b/(a+b)$, where a, b and c are the absorption coefficient, the scattering coefficient and the attenuation coefficient, respectively.

The new direction after collision is initially calculated in a local polar coordinate system that is determined with the z axis parallel to the incident photon direction. We choose the azimuth angle θ and scattering angle ϕ to represent the direction. The azimuth angle ϕ is considered to obey a uniform distribution between 0 and 2π, and the scattering angle θ is selected from a random distribution based on the Henyey–Greenstein function [18] which is specified by an anisotropy factor g. Then the new direction is converted to global coordinates.

The above processes is repeated until the photon reaches the boundary that is the ocean floor or the ocean surface. The ocean bottom is represented by a Lambert surface where photons are reemitted uniformly in all directions. When the photon reaches the atmosphere–ocean interface, we compare a random number with the transmissivity for the current angle of incidence in order to determine whether the photon is reflected or transmitted at the surface. The path of each photon is followed until the statistical weight falls below a predetermined number or the photon is transmitted at the interface. Now a new photon is launched until the total number of photons is achieved.

Because our model needs to consider a limited receiver field of view (FOV), to accelerate the calculation, an alternative is to use a procedure that analytically evaluates during the simulation the portion of the scattered light that goes directly from each collision point to the receiver [19].

In programming, the received echo signals including backscattered light and sea floor reflected signal are registered in an array, and the time interval between two adjacent array elements is the sample time. When a photon can be successfully received, its weight is added to the corresponding element which is decided by its arrival time. In the first stage, for pulse width 0, all the photons are supposed to be emitted at the same time.

2.2. Model for propagation of a realistic pulse

In this step, let us consider the simulation of a realistic pulse in one modulation period T_{m}. A T_{m} ns emitted pulse is divided into n uniform segments by a time interval Δt, where $n = T_{\mathrm{m}}/\Delta t$. Here, Δt is the sample time or resolution of the signal. Because the modulation frequency must be substantially greater than the cut-off frequency of the backscattered signal, i.e. of the order of GHz, in order to satisfy the Nyquist criterion, the sample time must be far less than 1 ns (0.01 ns typical). Supposing each simulated pulse consists of N_{pulse} photons, these N_{pulse} photons are divided into n segments according to the modulation waveform. The different waveform leads to a different calculation of N_i, where N_i is the photon number in the ith segment. Let us take for example squared and sinusoidal modulation.

For squared modulation, if $i \leqslant k$, where k which is relative to the duty ratio r can be given by $k = nr$, the photon number of the ith segment $N_i = N_{\mathrm{pulse}}/k$. If $k < i \leqslant n$, $N_i = 0$.

The case for sinusoidal modulation is slightly complicated, but N_i can be expressed by

$$N_i = [1 + \sin(2\pi f_{\mathrm{m}} \mathrm{i}\Delta t - \pi/2)]\Delta t f_{\mathrm{m}} N_{\mathrm{pulse}} \tag{1}$$

where $f_{\mathrm{m}} = 1/T_{\mathrm{m}}$ is the modulation frequency.

It is believed that the photons in the same segment are launched at the same time and the emitting time discrepancy of two adjacent segments is Δt; thereby, propagation of each segment in the atmosphere–ocean system can be simulated by the first stage, which is a Monte Carlo model for propagation of a 0-pulse-width light pulse. As mentioned previously, when the simulation for propagation of every segment is accomplished, an array storing the corresponding echo signal is acquired. These arrays are shifted according to the positions of their respective segments and accumulated to create a new array that stores the echo signal of a realistic pulse. We define that the ith element of array A is $A[i]$ where $i \geqslant 0$. Assuming that the echo signal of the jth segment is registered in array A_j and the summation of echo signals of the former j segments is stored in array B_j, obviously, B_1 is equal to A_1, and the ith element of B_1 is given by

$$B_1[i] = A_1[i]. \tag{2}$$

In the case of $j > 1$, if $i < j - 1$, the ith element of B_j can be easily given by

$$B_j[i] = B_{j-1}[i]. \tag{3}$$

If $i \geqslant j - 1$, the ith element of B_j can be recursively obtained by

$$B_j[i] = B_{j-1}[i] + A_j[i - j + 1]. \tag{4}$$

We repeat the above procedure from $j = 1$ to n. When $j = n$, the array B_n is the return signal of a single pulse.

2.3. Model for propagation of modulated pulses

Here we take account of the modulation case in which a radiofrequency subcarrier is superimposed on the transmitted optical pulse. For various modulation waveforms, the processing in this stage is the same, because the influence of the modulation waveform is considered in the previous stage.

We assume that the modulation pulse is a pulse train which is composed of m pulses and that total photon number

used in the simulation is N_{total}. Then the photon number contained in each pulse is easy to calculate, and we obtain $N_{\text{pulse}} = N_{\text{total}}/m$. The return signal of each single pulse in the train is emulated by the second stage, that is, the Monte Carlo simulation for propagation of a realistic pulse. The simulation result of each pulse is registered in a corresponding array. Similarly, these arrays are respectively shifted and then accumulated to form a new array representing the return signal of the modulated pulse. The relative offset s of the resulting arrays of two adjacent pulses is determined by the modulation period T_{m}, that is, by $s = T_{\text{m}}/\Delta t$. In detail, supposing that the return signal of the kth pulse in a pulse train is saved in array C_k and the summation of return signals of former k pulses is stored in array D_k, apparent when $k = 1$, D_1 is the same as C_1, and we obtain the ith element of D_1 by

$$D_1[i] = C_1[i]. \tag{5}$$

When $k > 1$, if $i < s(k-1)$, the ith element of array D_k is simply given by

$$D_k[i] = D_{k-1}[i]. \tag{6}$$

If $i \geqslant s(k-1)$, the ith element of array D_k is recursively expressed by

$$D_k[i] = D_{k-1}[i] + C_k[i - s(k-1)]. \tag{7}$$

We repeat the above procedure from $k = 1$ to m. When $k = m$, the array D_{m} is the final return signal of the modulated pulse.

The simulation program based on the model previously detailed is realized by using the C++ language. Through the program, several simulation experiments are performed to study the problems we are concerned with.

3. Design of signal processing model for receiver

For a modulated pulse bathymetric LIDAR system, the processing of the return signal is also different from that of a conventional LIDAR system due to its different detection mechanism. To better understand its signal processing method, first the backscattering frequency responses are calculated by our simulation program.

3.1. Calculations of backscattering transfer function

The backscattering transfer function can be computed from the water impulse response by taking the power spectrum. Since the pulse width of an impulse is zero, we only utilize the first stage stated in the above model to compute the backscattering impulse response from common parameters of ocean water. To compare with Pellen's water tank experimental study of seawater cut-off frequency [6, 7], the simulation is carried out with the same attenuation coefficients c of 0.46, 0.67 and 0.95 m^{-1}, and refractive index $n = 1.33$. The respective backscattering signals which are actually the impulse responses are simulated by our emulator program. Subsequently the corresponding frequency responses are obtained by computing the power spectrum of these impulse responses.

Figure 2 presents the backscattering frequency responses for $c = 0.46, 0.67$ and 0.95 m^{-1}. All intensities have been normalized. The plots in figure 2 show that the backscattering frequency response has a low-pass filter-like response, which enables us to estimate the cut-off frequency through our simulation program. The maximum cut-off frequency simulated at -3 dB is $f_{\text{c}} = 42$ MHz for $c = 0.95$ m^{-1}, which is in proximity to the published experimental one of about 40 MHz [6, 7]. The slightly variance between the two results is due to theoretical approximations and the different receiver parameters. In compliance with the tank experimental results [6, 7] and the values predicted from Mullen's model [5], the simulation results show that the cut-off frequency is lower for clear water. Hence the cut-off frequency of the backscattered signal is relatively low, i.e. below 100 MHz.

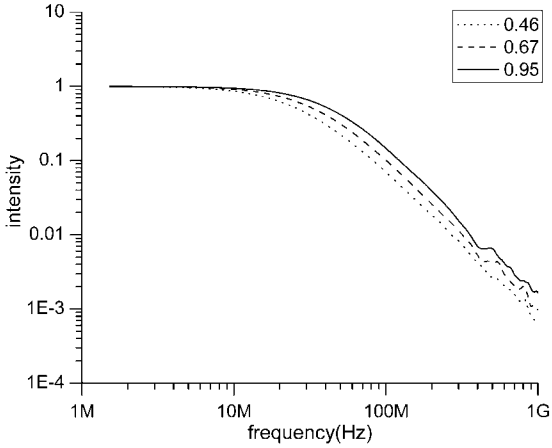

Figure 2. Backscattering frequency responses for $c = 0.46, 0.67, 0.95$ m^{-1} (log–log scale).

In contrast, it has been found that the underwater target remains relatively independent of frequency [5]. Therefore, to significantly reduce the backscattering clutter, one should use a modulation frequency substantially greater than this cut-off frequency, i.e. of the order of GHz, where the backscattering noise is diminished, but target reflections are unaffected.

3.2. Signal processing method

To reveal the target reflection hidden by backscattering, a narrow band filtering is used at the receiving end to filter out the low-frequency part of the return signal. In our simulation model, we performed a numerical narrow band filtering of the return signal by computing its cross-correlation with a sinusoidal signal generated at the modulation frequency, but the period number of the sinusoidal signal is limited to pulse number of the emitted pulse sequence.

The cross-correlation of signal $f(t)$ and $g(t)$ is defined by

$$C_{fg}(t) = \int_{\Re} f(\tau) \cdot g^*(\tau - t)\,\mathrm{d}\tau = f(t) * g^*(-t) \tag{8}$$

where $*$ denotes the convolution operator and $g^*(t)$ is the complex conjugate of $g(t)$. The cross-correlation is representative of the similarity between the two signals. Through the comparison of one signal portion to another shifted in time, we are able to detect hidden periodicity or to reveal a signal embedded in noise. For two uncorrelated signals, i.e. signal and noise, their cross-correlation is a

Table 1. Parameters of the simulation experiment.

Parameter name	Value
⟨WATER⟩	
Attenuation coefficient (m^{-1})	0.67, 0.85
Absorption coefficient (m^{-1})	0.1
Refractive index	1.33
Anisotropy factor g	0.9
⟨OBJECT⟩	
Albedo	0.1
Depth (m)	5
⟨RECEIVER⟩	
Aperture (m)	0.08
FOV (mrad)	20
⟨SOURCE⟩	
Modulation frequency (GHz)	1.5
Pulse width (ns)	3
Duty ratio (%)	50

constant which is equal to the product of their respective average value. Because of the sinus mean value equal to zero, the cross-correlation with the backscattering component is very weak, which enhances the target contrast.

4. Simulation results and discussion

4.1. Simulation of LIDAR return signal

Using the above-mentioned model for modulated pulse bathymetric LIDAR systems, we carried out a simulation experiment on underwater target detection. For the convenience of comparison between our simulation result and the published laboratory experimental result, the simulation incorporates the reported parameters of the tank experiment by Pellen *et al* [7], which are the modulation frequency $f_m = 1.5$ GHz, the pulse width $T = 3$ ns, the refractive index of water $n = 1.33$, and the attenuation coefficients c of 0.67 and 0.85 m^{-1}.

The anisotropy factor g is used to specify the Henyey–Greenstein function which mimics the angular dependence of light scattering. The parameter g is equal to the expectation value for $\cos(\theta)$, where θ is the scattering angle. The span of g is from -1 to 1. The closer the value of g is to 1, the more forward scattering is obtained, whereas the closer the value of g approaches -1, the more backward scattering is obtained. We can choose the value according to the scattering medium studied. Here, we chose $g = 0.9$, since the forward scattering is far more than the backward scattering for sea water.

Other required parameters such as FOV and the receiving aperture were mainly estimated from the ordinary LIDAR experimental set-up. It should be mentioned that the receiver geometry and the parameter g can be slightly adjusted to make the backscattering frequency responses simulated close to those measured in Pellen's experiment, or to make the calculated cut-off frequency approach the experimental one.

The various experimental parameters that were used in the simulation, including the receiver geometry, the optical parameters of water, are shown in table 1. Moreover, the emitted pulse sequence uses squared modulation.

The echo profiles of a 3 ns modulated pulse from a 5 m deep underwater target for $c = 0.67$ and 0.85 m^{-1} were calculated by Monte Carlo simulation of 10^6 photons. Figures 3 and 4 respectively depict the simulation results for $c = 0.67$ and 0.85 m^{-1}. The vertical ordinate represents the received light intensity, which is normalized by dividing every intensity value in the return signal by the maximum value. The return signal in figures 3 contains two main components that are the volume backscattering signal and the reflection on the target. The backscattering signal decreases with return time, and it exhibits a characteristic exponential decay when the vertical ordinate is transformed into log scale, as shown in the following section. As the attenuation coefficient for figure 4 was greater than for figure 3, the intensity of the target reflection relative to the water backscattering is lower in figure 4.

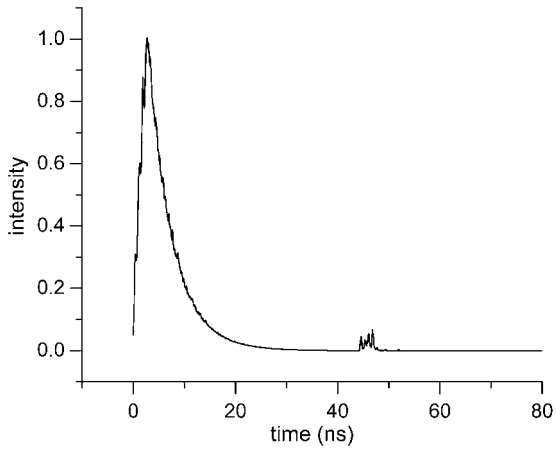

Figure 3. Return signal from a 5 m deep underwater target for $c = 0.67$ m^{-1}.

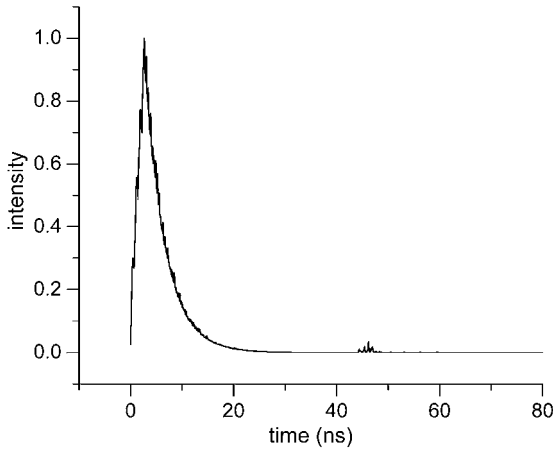

Figure 4. Return signal from a 5 m deep underwater target for $c = 0.85$ m^{-1}.

It is important to note that the modulated information is present in the target reflected signal, especially in figure 3, whereas the medium backscattering signal seems not to contain the modulated signal. So a narrow band pass filter at the modulation frequency must drastically reduce the backscattering clutter and not affect the target signal.

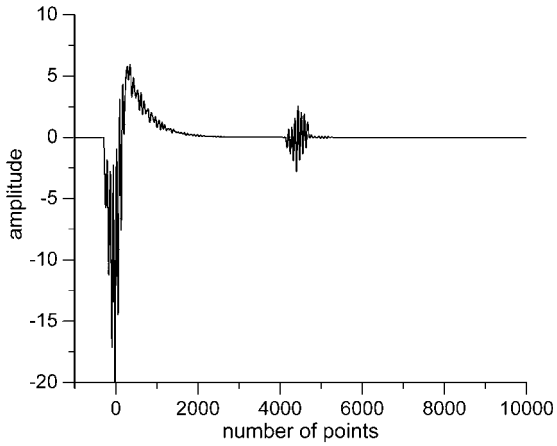

Figure 5. Cross-correlation result for $c = 0.67$ m^{-1} and a 5 m deep target.

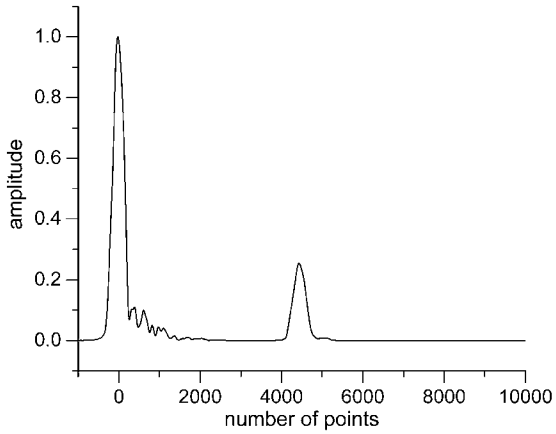

Figure 7. Filtering result deriving from cross-correlation result for $c = 0.67$ m^{-1} and target at 5 m depth.

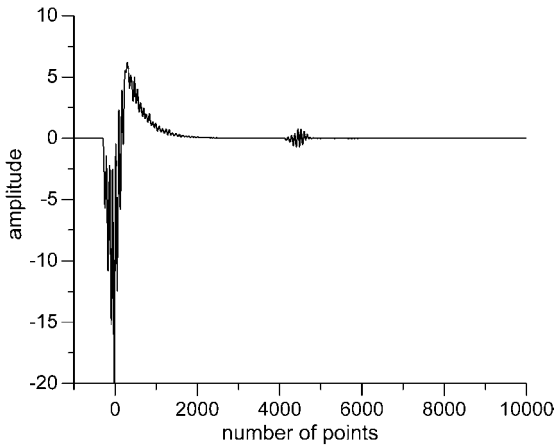

Figure 6. Cross-correlation result for $c = 0.85$ m^{-1} and a 5 m deep target.

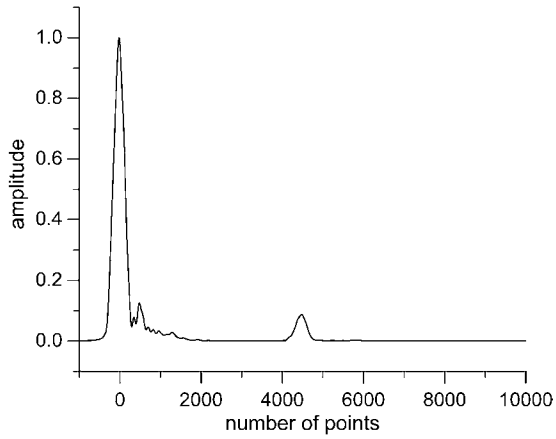

Figure 8. Filtering result deriving from cross-correlation result for $c = 0.85$ m^{-1} and target at 5 m depth.

4.2. Signal processing

4.2.1. Cross-correlation. As we previously detailed, the narrow-band filtering is implemented by cross-correlation. The cross-correlation of figures 3 and 4 with the sinusoidal signals results in figures 5 and 6, respectively.

In the two figures, the vertical ordinate represents the amplitude of the cross-correlation result, and the horizontal ordinate represents the resultant lag. Because in a return signal array the time interval of two adjacent array elements is the sample time Δt, one can simply transform a horizontal coordinate value into return time by multiplying this value by Δt. It should be noticed that this transform is limited to positive values, for minus time is null. A comparison of figures 3–6 shows that target contrast enhancement is achieved with the modulation approach. For example, in figure 4, the target echo on time recording of the backscattering signal is very small in comparison with the volume backscattering. Nevertheless, in figure 6, it is visible after the cross-correlation processing.

4.2.2. Filtering. One should note that high-frequency oscillations exist in the cross-correlation results. These oscillations indicate the high-frequency domain of the plots, which corresponds to cross-correlation echoes. Furthermore, the plot also includes the lower frequency domain which corresponds to the residual medium backscattering and low-frequency oscillations. To get a better target contrast, the two frequency domains are then respectively filtered. We adopt two FFT (fast Fourier transform) filters for digitally filtering data in the Fourier domain: low-pass and high-pass filters. First, the cross-correlation results were filtered by a high-pass filter. The residual medium backscattering and the low-frequency oscillations then disappeared. We then rectified and low-pass filtered the obtained signals. The results of this processing are respectively showed in figures 7 and 8; the amplitude is also normalized.

The plots in figures 7 and 8 clearly show that such a filtering make the target reflection more evident. In other words, such a filtering drastically reduced the backscattering clutter and greatly improved the underwater target contrast.

4.3. Comparison with experimental results

We may compare the plots in figures 3–8 with the corresponding ones obtained from Pellen's water tank

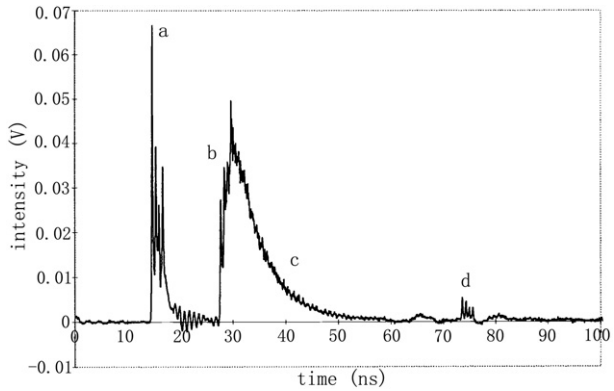

Figure 9. Experimental profile of backscattered signal from a 5 m deep underwater target for $c = 0.67$ m^{-1}.

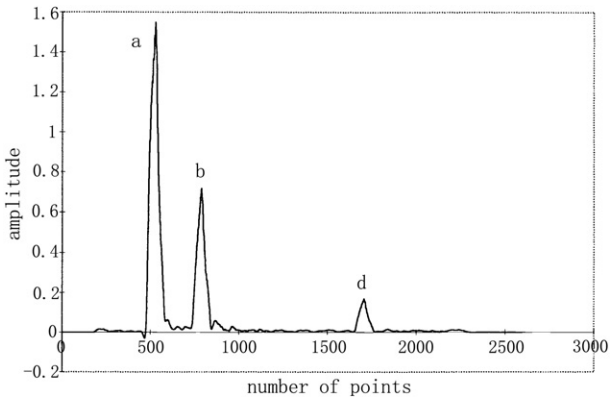

Figure 11. Experimental profile of filtering result for $c = 0.67$ m^{-1} and target at a 5 m depth.

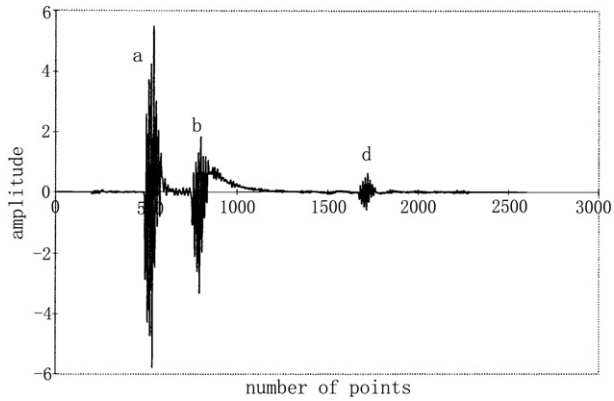

Figure 10. Experimental profile of cross-correlation result for $c = 0.67$ m^{-1} and target at a 5 m depth.

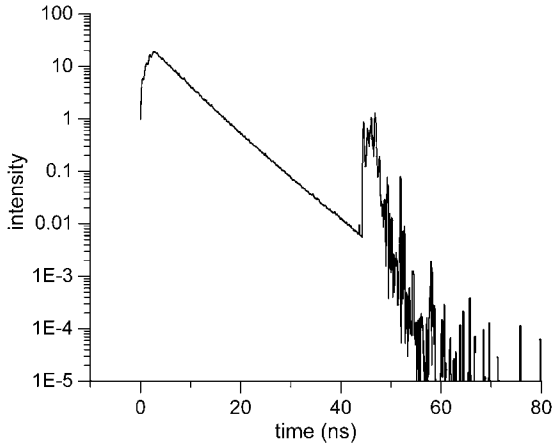

Figure 12. Return signal from a 5 m deep underwater target for $c = 0.67$ m^{-1} (log scale for intensity).

experiment in [7] so as to validate the ability of our simulation program in predicting experimental results. Taking example $c = 0.67$ m^{-1}, figure 9 displays the experimental shape of the backscattering signal from a target immersed at a 5 m depth [7]. The signal in figure 9 contains four main components: (a) the diffusion effect on the beam splitter mirror in the experimental set-up; (b) an echo due to the diffusion on the entrance window; (c) the volume backscattering signal; (d) the reflection on the immersed target. Apparently, for our comparison, the component (a) is negligible.

Figure 10 depicts the cross-correlation of the plot in figure 9 with the sinusoidal signal generated at the modulation frequency [7].

Figure 11 shows the filtering result of the plot in figure 10. Unlike the processing in our simulation, Pellen *et al* used a differential to obtain a high-pass filter [7].

It is noticed that figures 3, 5 and 7 depict the corresponding simulation plots for $c = 0.67$ m^{-1} and target at a 5 m depth. We can compare the two groups of plots by shape. The comparison reveals that the simulation results are similar to the experimental ones except for the diffusion effect on the mirror (a), respectively. In fact, the profiles simulated for $c = 0.85$ m^{-1} also resemble the corresponding experimental ones, but we shall not give them in order to reduce the length of the paper. The comparison validates the use of the simulation model for predicting experimental results.

4.4. Quantitative analysis of results

To quantifiably analyse the ability of the modulation detection scheme to reduce backscattering clutter and enhance the target contrast, we compare the plots obtained by the simulation in logarithmic coordinates. For instance, the logarithmic transformation results of plots in figures 3 and 7 are respectively shown in figures 12 and 13. To directly compare these two plots, we normalize the amplitude of the target reflection to 1, because the reflected signal from the underwater target is relatively independent of modulation frequency.

The plot in figure 12 shows that the backscattering signal indeed exhibits an exponential decay, as previously described. The plot in figure 13 approximately keeps this character. A comparison of the backscattering domains of these two plots shows that the effect of the narrow band pass filter at the modulation frequency seems to shift the backscattering portion downwards. That is, the backscattering clutter is reduced by approximately 19 dB optically, while the contrast of the target is increased by approximately 8 dB optically. These

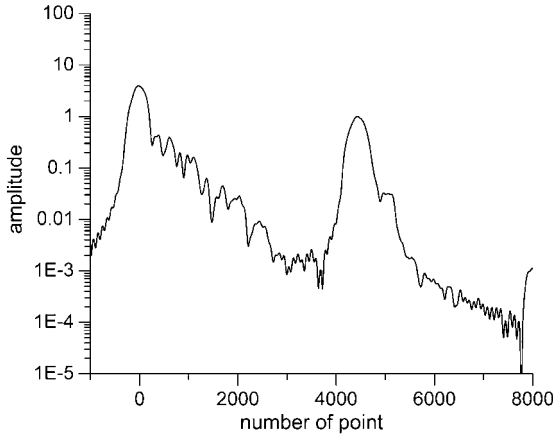

Figure 13. Filtering result deriving from cross-correlation result for $c = 0.67\ \mathrm{m}^{-1}$ and target at 5 m depth (log scale for amplitude).

two values exhibit more clearly the clutter reduction and the contrast enhancement. In addition, the two values are in relative agreement with Mullen's OMS experimental results that are respectively 17 and 5 dB [1]. This demonstrates the validity of our Monte Carlo simulation again from another point of view.

5. Conclusion

This paper has presented a Monte Carlo simulation model which incorporates the Monte Carlo technique, cross-correlation and numerical filtering to emulate a modulated pulse bathymetric LIDAR system. The emulator program based on the model is also developed. The simulation results exhibit that the modulation scheme indeed suppresses volume backscattering and improves the detection of underwater targets. Furthermore, a comparison of the computer simulation and the published experimental results exhibits a reasonable agreement, which verifies the simulation model.

Moreover, because various parameters including the water optical properties, the modulation parameters and transmitter/receiver geometries can be conveniently changed in the simulation, the simulation program is able to depict laboratory or actual ocean environment results in all kinds of conditions, and can help optimizing the transmitter and receiver configuration. In future, we hope to improve the simulation program and perform more simulation experiments to understand better the effect of various parameters on the modulated pulse LIDAR system performance.

Acknowledgment

The authors wish to thank Wei Li for her help in preparing the manuscript.

References

[1] Mullen L, Herczfeld P R and Contarino V M 1994 Modulated pulse LIDAR system for shallow underwater target detection *Proc. IEEE Oceans Engineering for Today's Technology and Tomorrow's Preservation* vol 1, pp 835–9

[2] Pellen F, Olivard P, Guern Y, Cariou J and Lotrian J 2000 Radar modulation on optical carrier for target detection in sea-water *Proc. IEEE Lasers and Electro-Optics Europe* p 1

[3] Mullen L, Contarino V M, Laux A, Concannon B and Davis J 1999 Application of hybrid lidar–radar technology to a laser line scanner system *CLEO '99: Conf. IEEE Lasers and Electro-Optics* p 553

[4] Mullen L and Herczfeld P R 1994 Application of radar technology to aerial LIDAR systems *Proc. IEEE Microwave Symposium Digest* vol 1, pp 175–8

[5] Mullen L, Vieira A J C, Herczfeld P R and Contarino V M 1995 Application of RADAR technology to aerial LIDAR systems for enhancement of shallow underwater target detection *IEEE Trans. Microw. Theory Tech.* **43** 2370–7

[6] Pellen F, Intes X, Olivard P, Guern Y, Cariou J and Lotrian J 2000 Determination of sea-water cut-off frequency by backscattering transfer function measurement *J. Phys. D: Appl. Phys.* **33** 349–54

[7] Pellen F, Olivard P, Guern Y, Cariou J and Lotrian J 2002 Radiofrequency modulation on optical carrier for target detection enhancement in sea-water *Proc. SPIE Ocean Optics: Remote Sensing and Underwater Imaging* vol 4488, pp 13–24

[8] Mullen L, Contarino V M and Herczfeld P R 1996 Hybrid lidar–radar ocean experiment *IEEE Trans. Microw. Theory Tech.* **44** 2703–10

[9] Mullen L, Contarino V M and Herczfeld P R 2000 Hybrid lidar–radar: seeing through the scatter *IEEE Microw. Mag.* **1** 42–8

[10] Mullen L and Herczfeld P R 1996 Full scale hybrid lidar–radar system *Proc. IEEE Microwave Symposium Digest* vol 3, pp 1559–62

[11] Mullen L, Zege P E, Katsev I L and Prikhach A S 2002 Modulated lidar system: experiment vs. theory *Proc. SPIE Ocean Optics: Remote Sensing and Underwater Imaging* vol 4488, pp 25–35

[12] Plass G N and Kattawar G W 1968 Monte Carlo calculations of light scattering from clouds *Appl. Opt.* **7** 415–9

[13] Plass G N and Kattawar G W 1969 Radiative transfer in an atmosphere–ocean system *Appl. Opt.* **8** 455–66

[14] Bergougnoux L, Misguich-Ripault J, Firpo J-L and Andre J 1996 Monte Carlo calculation of backscattered light intensity by suspension: comparison with experimental data *Appl. Opt.* **35** 1735–41

[15] Funk C J 1973 Multiple scattering calculations of light propagation in ocean water *Appl. Opt.* **12** 301–5

[16] Tinet E, Avrillier S and Tualle J M 1996 Fast semianalytical Monte Carlo simulation for time-resolved light propagation in turbid media *J. Opt. Soc. Am.* A **13** 1903–15

[17] Liu Q, Yang K, Liu J, Tan D, Gao Y and Yu L 2004 Simulation by Monte Carlo method of effect of lidar's fields of view to echo signals *Proc. SPIE—Opt. Design Testing II* vol 5638, pp 937–40

[18] Toublanc D 1996 Henyey–Greenstein and Mie phase functions in Monte Carlo radiative transfer computations *Appl. Opt.* **35** 3270–4

[19] Poole L R, Venable D D and Campbell J W 1981 Semianalytic Monte Carlo radiative transfer model for oceanographic lidar systems *Appl. Opt.* **20** 3653–6